cancers

Article

Dynamic PD-L1 Regulation Shapes Tumor Immune Escape and Response to Immunotherapy

Bruce Pell [1,*], Aigerim Kalizhanova [2], Aisha Tursynkozha [3], Denise Dengi [4], Ardak Kashkynbayev [2] and Yang Kuang [5]

[1] Department of Mathematics and Computer Science, Lawrence Technological University, Southfield, MI 48075, USA
[2] Department of Mathematics, Nazarbayev University, 010000 Astana, Kazakhstan; aigerim.kalizhanova@nu.edu.kz (A.K.); ardak.kashkynbayev@nu.edu.kz (A.K.)
[3] Department of Artificial Intelligence and Data Science, Astana IT University, 010000 Astana, Kazakhstan; aisha.tursynkozha@nu.edu.kz
[4] Department of Mathematics, University of California Berkeley, Berkeley, CA 94720, USA; ddengi@berkeley.edu
[5] School of Mathematical and Statistical Sciences, Arizona State University, Tempe, AZ 85287, USA; kuang@asu.edu
* Correspondence: bpell@ltu.edu

Simple Summary

Combination cancer immunotherapy, such as pairing the immunostimulant NHS-muIL12 with the PD-L1 blocker Avelumab, holds considerable promise, but tumors often develop adaptive resistance. We investigate a mechanism of treatment failure in which NHS-muIL12 boosts immune activity while simultaneously inducing tumor PD-L1 upregulation, reducing Avelumab's efficacy. We developed a mathematical model to capture this interaction, providing a unified framework for both treatment success and failure. By reparameterizing key rates controlling PD-L1 expression, the model reproduced outcomes across two tumor types. This work highlights the utility of mathematical modeling for testing mechanistic hypotheses, quantifying factors underlying therapeutic response, and guiding improved dosing strategies.

Abstract

Background: A major challenge in cancer treatment is the ability of tumor cells to adapt to immunotherapy through immune escape, often mediated by the PD-1/PD-L1 pathway. To investigate this, we adapted an ordinary differential equation model of combination therapy, incorporating the dynamics of the immune checkpoint inhibitor Avelumab and the immunostimulant NHS-muIL12. **Methods**: Using literature-derived parameter values, we refitted a single parameter across therapies, which showed that PD-L1 expression increased with immunotherapy, while Avelumab blocked its functional signaling, preventing PD-L1 from suppressing T-cell activity. Incorporating therapy-dependent, dynamically regulated PD-L1 expression enabled a biologically grounded mechanism to reproduce experimental observations, leading us to formulate PD-L1 tumor expression as a dynamic variable (ϵ) and providing a mechanistic basis for both therapeutic synergy and treatment failure. **Results**: We validated this mechanistic framework by showing that the distinct outcomes observed in two independent cancer datasets (EMT-6 and MC38) can be captured by the same model structure, differing only in the parameterization of tumor-specific parameters and PD-L1 regulatory dynamics. Our results indicate that tumor resistance is linked to dose-dependent upregulation of PD-L1 following NHS-muIL12 treatment, explaining treatment failure, while PD-1/PD-L1 blockade in combination therapy enables effective antitumor

check for updates

Academic Editor: Hermann B. Frieboes

Received: 1 October 2025
Revised: 13 November 2025
Accepted: 25 November 2025
Published: 27 November 2025

Citation: Pell, B.; Kalizhanova, A.; Tursynkozha, A.; Dengi, D.; Kashkynbayev, A.; Kuang, Y. Dynamic PD-L1 Regulation Shapes Tumor Immune Escape and Response to Immunotherapy. *Cancers* **2025**, *17*, 3803. https://doi.org/10.3390/cancers17233803

Copyright: © 2025 by the authors. Licensee MDPI, Basel, Switzerland. This article is an open access article distributed under the terms and conditions of the Creative Commons Attribution (CC BY) license (https://creativecommons.org/licenses/by/4.0/).

immune responses. **Conclusions**: This work provides a validated mechanistic framework for adaptive resistance in combination immunotherapy. Quantified parameter differences between responder and non-responder phenotypes enable clearer biological interpretation and support the development of predictive tools for optimizing treatment strategies.

Keywords: cancer immunotherapy; modeling; differential equations; PD-L1; adaptive immune response; math model; immunostimulant

1. Introduction

Cancerous tumors are not static entities but dynamically evolve under immune and therapeutic pressure, often developing sophisticated strategies to evade immune surveillance [1–3]. Understanding these adaptive mechanisms, particularly the intricate regulation of immune checkpoints like Programmed Cell Death Protein 1 (PD-1) or its ligand (PD-L1), is important for overcoming resistance to modern immunotherapies and for generating personalized treatment plans for patients [4–6]. The PD-1/PD-L1 signaling axis functions as a regulator of tumor immunity by suppressing T-cell activation, proliferation, and cytotoxic capacity [7]. Activated T-cells express the PD-1 receptor, and when it binds to its ligand, PD-L1, it delivers an inhibitory signal that deactivates the T-cell. Many cancers have co-opted this natural mechanism to evade the immune system by overexpressing PD-L1 on their surface, essentially neutralizing attacking T-cells [8].

The development of immune checkpoint inhibitors, which are monoclonal antibodies that physically block the interaction between PD-1 and PD-L1, has revolutionized cancer therapy [4,8]. Avelumab is an immunotherapy drug that acts as an immune checkpoint inhibitor to treat specific types of advanced cancer, including Merkel cell carcinoma, urothelial cancer, and renal cell carcinoma [9,10]. By binding to PD-L1, Avelumab blocks its interaction with the PD-1 receptor on T-cells, thereby preventing the deactivation of the antitumor immune response and effectively allowing cytotoxic T-lymphocytes to kill cancer cells [11]. While effective, checkpoint blockade alone often fails due to insufficient immune activation within the tumor microenvironment. For this reason, combination strategies that pair checkpoint inhibition with immunostimulatory agents have gained interest. One such agent is NHS-muIL12, a tumor-targeting immunocytokine that combines a tumor-targeting antibody with the immune-stimulating cytokine interleukin-12 (IL-12) [12]. IL-12 is a potent cytokine that stimulates the proliferation and activation of T-cells and Natural Killer (NK) cells [13]. Preclinical studies demonstrated that NHS-muIL12 increases immune infiltration and activity, while Avelumab prevents tumor-mediated suppression, leading to synergistic anti-tumor effects [14]. See Figure 1 for a schematic illustration of the main dynamics.

Mathematical modeling has emerged as a powerful tool to provide novel insight into cancer biology, tumor growth, and treatment response [15–18]. A comprehensive coverage of these topics can be found in Kuang et al. [19]. These quantitative frameworks are essential for deciphering the intricate, non-linear interactions between cancer cells, diverse immune populations, and therapeutic treatments, which are often challenging to isolate and measure experimentally [20,21]. Since mathematical models can be designed with specific mechanisms and pathways in mind, they provide a way to generate testable, data-driven hypotheses and optimize treatment strategies when parameterized to data [22–26]. For example, Meade et al. used a mathematical model of prostate cancer to develop novel indicators of treatment failure. Their work, based on an evolutionary perspective, led to the hypothesis that the ratio of androgen to prostate-specific antigen (PSA) could serve as a powerful prognostic biomarker for predicting resistance to therapy [24,25].

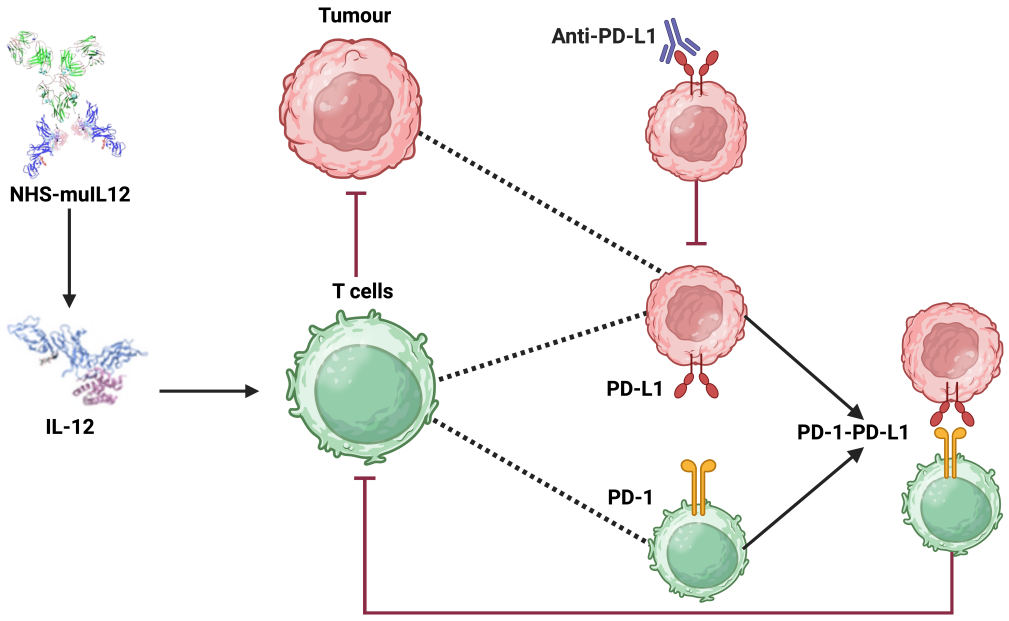


Figure 1. Schematic illustration of the synergistic antitumor mechanisms of NHS-muIL12 and anti-PD-L1 (Avelumab) checkpoint blockade within the tumor microenvironment. The diagram shows how NHS-muIL12 delivers IL-12 to promote T-cell activation, while anti-PD-L1 antibody therapy overcomes tumor-induced immune suppression by disrupting the PD-1/PD-L1 axis. Created in BioRender https://biorender.com/4yxwllp (accessed on 23 September 2025).

In a significant effort to understand the intricate dynamics governing tumor cell proliferation, immune responses, and the balance of therapeutic interventions, Nikolopoulou et al. constructed a mathematical model to investigate the enhanced antitumor efficacy observed with NHS-muIL12 and Avelumab combination therapy in preclinical cancer models [14,27]. In addition to analyzing the model, they found by using numerical simulations that this combination therapy requires only about one-third of the individual drug doses for tumor control compared to monotherapy.

In their simulation studies, they rigorously estimated parameter values from the literature and the remaining parameters were estimated by fitting the model to cancer treatment experiments that were conducted on mice in [14]. These experiments included the following: (a) Isotype control (no drug); (b) NHS-muIL12 (2 μg); (c) NHS-muIL12 (10 μg); (d) Avelumab (200 μg); (e) Avelumab (200 μg) and NHS-muIL12 (2 μg); (f) Avelumab (200 μg) and NHS-muIL12 (10 μg). BALB/c mice bearing orthotopic EMT-6 tumors (100 mm^3) were treated with Avelumab on days 0, 3, and 6, while NHS-muIL12 was administered as a single dose on day 0. Model fitting was systematic in the sense that they sequentially fit the model to data using more complexity as more treatments were introduced. Specifically, they used the no-drug case to estimate the proliferation rate of the tumor cells (r) and the kill rate of tumor cells by T-cells (η). From there, they estimated K_{A_2} by fitting the model to the NHS-muIL12 (2 μg) data and similarly they estimated K_{A_1} using the Avelumab (200 μg) data.

While the model by Nikolopoulou et al. provides a valuable framework, it fails to recapitulate the non-monotonic dynamics observed in the low-dose combination therapy. In this study, we posit that this discrepancy arises from the model's assumption of a constant PD-L1 tumor expression propensity, ϵ. We present an iterative model refinement, resulting in a model with a dynamic ϵ that successfully explains these complex dynamics. This work provides a quantitative framework for understanding adaptive immune resistance and establishes a platform for developing novel, model-derived biomarkers to predict therapeutic outcomes. Figure 2 shows the model with treatment-dependent ϵ, illustrating

that allowing ϵ to vary across treatments both improves the model fit and captures tumor adaptation to the immune response under different therapies.

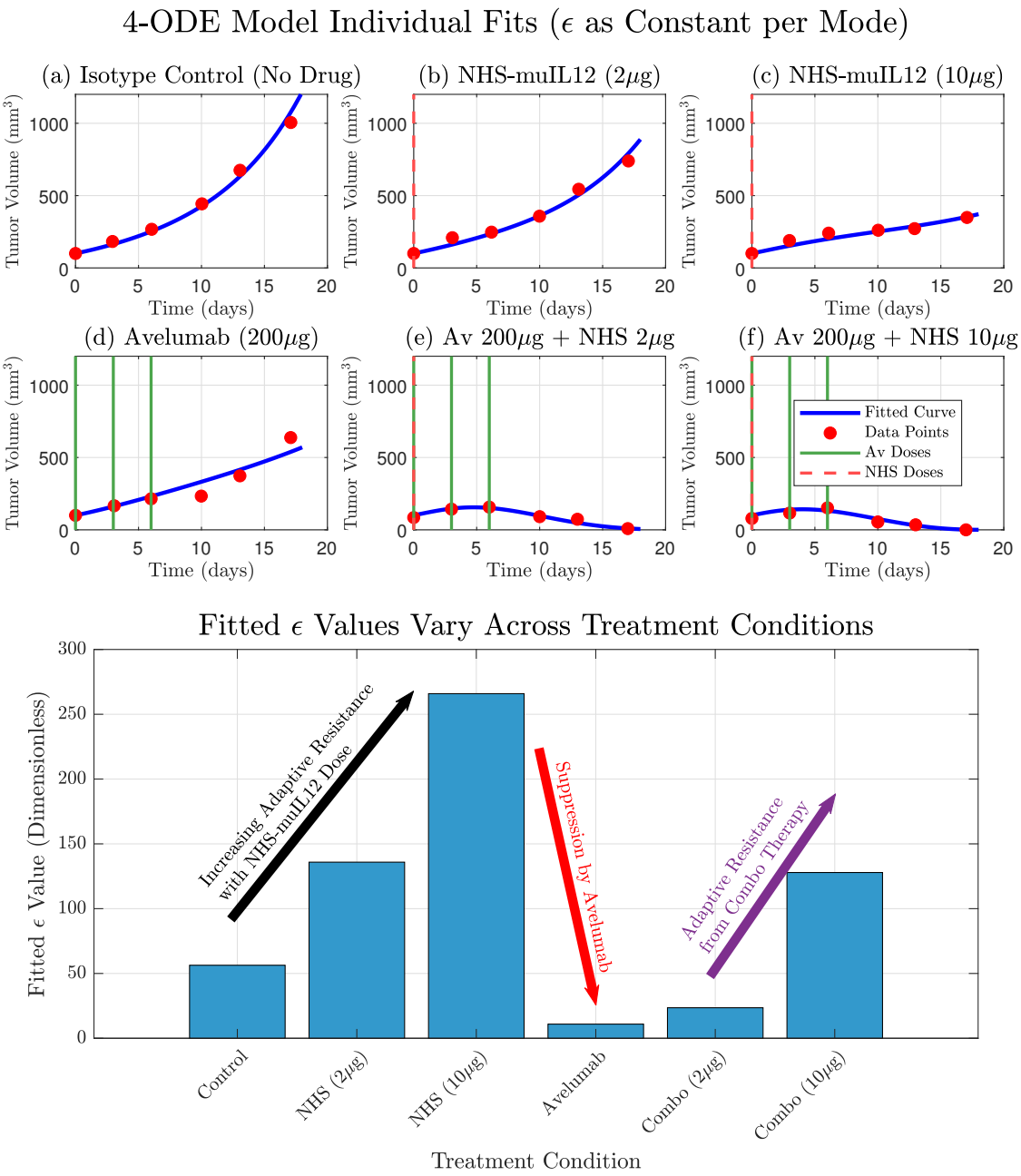


Figure 2. The original model by Nikolopoulou et al. adapted with therapy-specific PD-L1 expression (ϵ) accurately recapitulates experimental data and reveals the dynamics of adaptive resistance. (**Top**) The model's simulated tumor volume (blue curves) shows a good fit to the experimental data (red circles) for all six treatment conditions. This fit was achieved by treating ϵ as a constant parameter that was individually fitted for each specific therapy. (**Bottom**) The resulting fitted values for ϵ are displayed for each condition. The values show a clear dose-dependent upregulation of ϵ in response to NHS-muIL12 monotherapy, a hallmark of adaptive resistance. Conversely, therapies including Avelumab show a strong suppression of the effective ϵ value, with a slight increase in the combination therapies due to the presence of NHS-muIL12.

2. Materials and Methods

2.1. Formulation of the Mathematical Model

We introduce the cancer treatment model first proposed by Nikolopoulou et al., who considered the micro tumor environment consisting of tumor cells and activated T-cells. Their mathematical model portrayed in Quick Guide 1 describes the interaction between tumor cells, activated T-cells, the anti–PD-L1 antibody Avelumab, and the immunostimulant NHS-muIL12. What follows is a narrative summary of the equations and assumptions.

Quick Guide 1: Original Model Equations and Assumptions

Here, we summarize the model from Nikolopoulou et al. [27], which we will adapt for this study. The model simplifies the tumor microenvironment to consist of two primary interacting cell populations: tumor cells, with volume $V(t)$ (mm^3), and effector T-cells, with volume $T(t)$ (mm^3). The model also tracks the concentration of the two therapeutic agents: the anti-PD-L1 antibody Avelumab, $A_1(t)$, and the immunocytokine NHS-muIL12, $A_2(t)$. The dynamics of these populations and agents are governed by the following system of ordinary differential equations:

$$\frac{dV}{dt} = rV - \eta VT, \qquad \frac{dA_1}{dt} = \gamma_1(t) - d_{A_1}A_1,$$
$$\frac{dT}{dt} = F(V, T, A_1, A_2) - d_T T, \qquad \frac{dA_2}{dt} = \gamma_2(t) - d_{A_2}A_2.$$

The top equation in the left column describes tumor growth, which is assumed to grow at an exponential rate (intrinsic growth rate r), but is reduced by T-cell-mediated killing at a rate η based on the law of mass action. The bottom left equation models the rate of change of the T-cell population, where the function F represents stimulation by the tumor and drug treatments, and decays at a rate d_T. Finally, the pharmacokinetics of the anti-PD-L1 antibody Avelumab (A_1) and the immunostimulant NHS-muIL12 (A_2) are modeled, where $\gamma_i(t)$ terms represent drug administration and d_{A_1} and d_{A_2} are the respective clearance rates.
The T-cell activation function F quantifies the production and stimulation of the immune system and is given by:

$$F(V, T, A_1, A_2) = \left(\delta + \lambda_{T12} T \frac{c_2 A_2}{K_{A_2} + c_2 A_2}\right)\left(\frac{1}{1 + Q(V, T, A_1)/K_{TQ}}\right)$$

where $Q(V, T, A_1)$ quantifies the effective inhibition via the PD-1/PD-L1 complex. The first term in the parentheses represents the basal production and stimulatory component. In particular, F increases with increasing values of the immunostimulate A_2 which is assumed to follow Michaelis-Menten dynamics and is proportional to T. Furthermore, it is assumed that there is a background production at rate δ. The second term in the product represents the immunosuppressive effect of the PD-1/PD-L1 immune checkpoint, and how it is reversed by the checkpoint inhibitor Avelumab (A_1), through the PD-1/PD-L1 complex, Q. As Q increases, this second term gets smaller and hence reduces the value for F. Q is a function dependent on V, T and A_1 and has the following form given by

$$Q(V, T, A_1) = \sigma \rho_P \rho_L T(T + \epsilon V)(1 - \phi(A_1)) \quad \text{with} \quad \phi(A_1) = \frac{c_1 A_1}{c_1 A_1 + K_{A_1}},$$

where σ represents the fraction of complex association and dissociation, which was derived in [27]. It assumes that the complex Q increases proportionally to T and V, but decreases with more anti-PD-L1 antibody A_1 through the term $1 - \phi$, which assumes ϕ is a Michaelis–Menten response curve. ρ_P and ρ_L are the expression levels of PD-1 and PD-L1, respectively. In this model, ϵ represents the functional immunosuppressive strength of the tumor, capturing its net ability to evade the immune system rather than reflecting the literal PD-L1 concentration or direct molecular count. For a more detailed description of the model and parameter meanings, see [27] and Table A1.

In this model, tumor cells (mm^3) grow exponentially but are counteracted by T-cell-mediated killing. We justify using exponential growth as a baseline for tumor growth, as it accurately captures the growth curve observed in the control group data (Isotype Control, Figure 3) and is a common way of modeling early cancer proliferation [28], while the T-cell-mediated killing term employs a standard law of mass action formulation foundational to the field [29]. T-cell population (mm^3) increases in response to both tumor antigen stimulation and the immune-boosting effects of NHS-muIL12, while also undergoing natural turnover. The two drugs, Avelumab and NHS-muIL12, are modeled through their pharmacokinetics, with infusion inputs ($\gamma_i(t)$) and clearance terms (d_{A_i}).

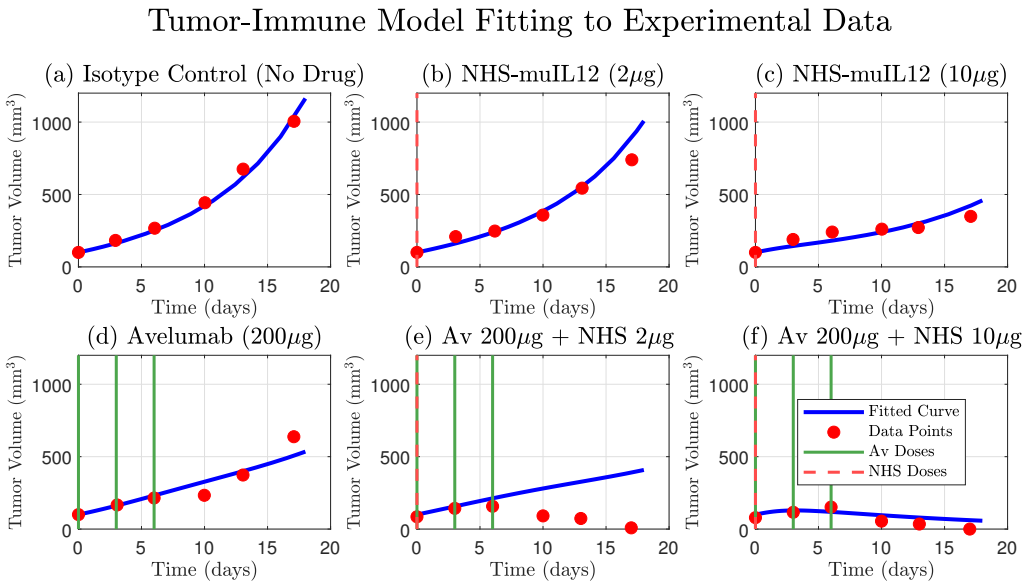


Figure 3. Comparison of the original 4-ODE model simulation against experimental tumor growth data. The model, parameterized as in Nikolopoulou et al. [27], accurately describes the tumor growth kinetics for the isotype control group (**a**) and the partial efficacy of the NHS-muIL12 (**b**,**c**) and Avelumab (**d**) monotherapies. The simulated tumor volume (blue curve) is shown against the experimental data (red circles). The model also captures the strong synergistic effect and tumor regression observed in the high-dose combination therapy (**f**). However, a key finding is the model's inability to reproduce the tumor dynamics seen in the low-dose combination therapy data (**e**), where the tumor volume initially increases before decreasing. This discrepancy highlights a limitation in the original model formulation and suggests that a key biological mechanism is not being accounted for (compare with Figure 2). Dosing schedules for Avelumab and NHS-muIL12 are indicated by solid green and dashed red lines, respectively.

The key features of the model are the mechanistic approaches to immune stimulation and immune evasion (found in the F function, see Quick Guide 1). T-cells are produced at a basal rate (δ) and stimulated by the presence of NHS-muIL12 (A_2) in the tumor microenvironment. The stimulation rate is assumed to be proportional to the T-cell population and NHS-muIL12 dosage, whereas T-cell basal production is assumed to be constant. The former term is of Michaelis–Menten form to indicate the saturated effects of the immune response via stimulation by NHS-muIL12 [30]. To incorporate immune evasion, the model temporally tracks the amount of PD-1/PD-L1 complex, Q, which is assumed to be generated from T-cells and tumor cells, but decreases with the anti PD-L1 agent Avelumab. In particular, the model assumes that PD-1 is expressed on the surface of T-cells and PD-L1 is expressed by both T-cell and tumor cell surfaces. We are interested in the latter because this enables the tumors' ability to evolve and evade the immune system. For a more detailed model, its formulation and explanations can be found in [27] and are summarized in Quick Guide 1.

2.2. Experiment Data

Xu et al. rigorously investigated the antitumor efficacy of NHS-muIL12 and Avelumab, both as single agents and in combination, across two distinct preclinical cancer models with the goal of determining whether combination therapy with NHS-muIL12 and the anti-PD-L1 antibody Avelumab can enhance antitumor efficacy in preclinical models relative to monotherapies [14]. In particular, to generate the EMT-6 tumor data, BALB/c mice ($n = 8$ mice/group) were inoculated with 0.5×10^6 EMT-6 tumor cells orthotopically in the mammary fat pad. Mice were randomized into treatment groups when tumors reached the desired volume (day 0) and treatment was initiated on day 0 [14]. Avelumab or isotype control were injected intravenously on days 0, 3, and 6 for EMT-6 tumor-bearing mice. NHS-muIL12 was injected as a single subcutaneous dose on day 0 [14].

Tumor volume data were obtained from digitizing the data from Figure 1B of Xu et al. using PlotDigitizer (https://plotdigitizer.com/app (accessed on 18 June 2025)) [14,31]. The experiment data for the high-dose combination therapy (Mode 6) was reported in the original study [14] to exhibit a bimodal response. In particular, 7 of 8 mice (87.5%) resulted in complete tumor regression, while 1 mouse did not respond to treatment. Fitting a deterministic model to the mean of all 8 mice would be inappropriate, as this composite average represents the bimodal distribution (7 treatment success and 1 failure) and not a representative biological trajectory.

Therefore, to mechanistically investigate the primary, synergistic curative interaction, we have decided to use a dataset, which represents the mean of the 7 mice (87.5%) that exhibited complete tumor regression in the high-dose combination therapy case. A comparative analysis, detailed in Supplementary Figure S1 and Table S1, confirms that a single global model provides a superior fit to this dataset versus the composite 8-mouse mean, validating this separation.

2.3. Updated Parameter Values

To understand tumor evolution and adaptation, we take the original model (see Quick Guide 1) and fit ϵ across the different therapies. In this way, we can understand the tumor's adaptive response as different treatments are used.

We use updated parameter values either found from the literature or values that were initially derived by Nikolopoulou et al. but were not used. In particular, we take $\lambda_{T8I12} = 4.15\ \text{day}^{-1}$ as was initially used by Lai and Friedman to account for $CD8^+$ T-cells [32]. In addition, we update the degradation rates for Avelumab (A_1) and NHS-muIL12 (A_2), since the original parameters were derived from human data, as well as the

experiments Xu et al. applied on mice. Murine-specific literature provides the following more accurate values:

- Avelumab: half-life ≈ 44.6 h $= 1.86$ days $\implies d_{A_1} \approx 0.3726$ day^{-1} [33].
- NHS-muIL12: half-life ≈ 9.5 days $\implies d_{A_2} \approx 0.0730$ day^{-1} [34].

Lastly, we used the original values $K_{A_1} = 1 \times 10^{-13}$ and $K_{A_2} = 7 \times 10^{-14}$ that were derived from the literature values in [27]. We summarize the new parameter list in Table A1.

2.4. Model Refinement: Drug- and Tumor Size-Dependent ϵ

While some tumors may have a baseline level of PD-L1 expression, it is not a fixed property. The tumor's upregulation of PD-L1 is a defensive counter-adaptation. By increasing PD-L1 expression, the tumor can evade the very T-cells that were activated to attack it, creating a negative feedback loop that suppresses the immune response. A constant ϵ would completely ignore this crucial dynamic feedback, leading to an oversimplified and potentially inaccurate representation of the system's dynamics, particularly for combination therapies.

To capture this behavior, we develop a differential equation for ϵ that depends on tumor volume V, drug treatments A_1, A_2, and itself, ϵ. The dynamic ϵ is designed to quantitatively represent the well-documented biological mechanism of adaptive immune resistance, whereby tumor cells upregulate PD-L1 in response to IFN-γ secreted by effector T-cells [13,35]. We chose to link PD-L1 upregulation directly to the presence of NHS-muIL12 rather than explicitly modeling the intermediate IFN-γ step, as this simpler formulation is more robust and avoids further parameter identifiability issues while still capturing the essential dynamics. For a model that includes this pathway, we point interested readers to work by Liao et al. [36]. We again provide a narrative description of the ϵ differential equation equation below.

We assume that dynamic PD-L1 expression increases at a rate that is proportional to tumor size and saturates at a maximum volume [37,38]. In addition, PD-L1 naturally decays over time, and drug-mediated degradation or suppression by Avelumab can further reduce its levels [39,40]. We assume that the former follows an exponential decay while the latter follows a saturation function given by a Michaelis–Menten equation. Building on our assumption from the model where ϵ was held constant (see Figure 2), we further assume that ϵ increases with NHS-muIL12 and that PD-L1 expression increases as an adaptive response by tumor cells to immunostimulants [14]. For a more detailed explanation of the derivation for this governing equation, we point interested readers to Quick Guide 2.

Quick Guide 2: Dynamic PD-L1 Incorporation

To account for the adaptive nature of the tumor's PD-L1 expression, we introduced a fifth ordinary differential equation to govern the dynamics of the state variable ϵ. The rate of change of ϵ is modeled as a balance between production and degradation forces:

$$\frac{d\epsilon}{dt} = \begin{matrix}\text{Basal}\\ \text{Expression}\end{matrix} + \begin{matrix}\text{Drug-Induced}\\ \text{Expression}\end{matrix} - \begin{matrix}\text{Drug-Induced}\\ \text{Degradation}\end{matrix} - \begin{matrix}\text{Natural}\\ \text{Degradation}\end{matrix}.$$

We assume that tumors possess a basal production rate of PD-L1 expression that is independent of external stimulation. Here, that rate follows Michaelis–Menten

dynamics, where the production rate increases with tumor size but approaches a maximum:

$$k_{basal}\frac{V}{K_V+V},$$

where k_{basal} represents the maximum production rate of PD-L1 from tumor cells and K_V is the half-saturation constant.

A fundamental mechanism of tumor immune escape is the upregulation of PD-L1 in response to an active antitumor immune attack. This process is primarily driven by pro-inflammatory cytokines, most notably interferon-gamma (IFN-γ), which is secreted by activated T-cells upon tumor antigen recognition. The PD-L1 production rate is modeled as being stimulated by NHS-muIL12 (A_2) in a tumor size-dependent manner, representing IFN-γ-mediated upregulation. This formulation captures adaptive immune resistance, in which immune-activating signals from the drug induce PD-L1 expression as a tumor defense mechanism. Based on this discussion, we assume functional forms that follow a saturation curve for both A_2 and V:

$$\alpha_{A_2}\frac{V}{K_V+V}\frac{c_2A_2}{K_{A_2}+c_2A_2}.$$

where K_ϵ and K_{A_2} are the half-saturation constants for V and A_2, respectively, and α_{A_2} represents the maximum rate of PD-L1 production by NHS-muIL12 stimulation. Avelumab is a monoclonal antibody that specifically binds to the PD-L1 protein on cancer cells. By doing so, it prevents PD-L1 from attaching to the PD-1 receptor on T-cells, which would normally send an inhibitory signal to deactivate them. This blockade allows the T-cells to remain active and effectively target and destroy the tumor cells. To this end, we assume the drug-mediated suppression of PD-L1 by Avelumab (A_1) is given by the following:

$$\alpha_{A_1}\frac{c_1A_1}{K_{A_1}+c_1A_1}\epsilon$$

where c_1 and K_{A_1} are defined as before, and α_{A_1} represents the maximum rate of drug-mediated suppression of PD-L1 by Avelumab.

Finally, we assume that tumor-derived PD-L1 expression decays at rate d_ϵ. The governing equation for the change in tumor PD-L1 expression level (ϵ) over time is

$$\frac{d\epsilon}{dt}=\underbrace{k_{basal}\frac{V}{K_V+V}}_{\substack{\text{Basal rate of}\\ \text{production}}}+\underbrace{\alpha_{A_2}\frac{V}{K_V+V}\frac{c_2A_2}{K_{A_2}+c_2A_2}}_{\text{Activation of }\epsilon\text{ by }A_2}-\underbrace{\alpha_{A_1}\frac{c_1A_1}{K_{A_1}+c_1A_1}\epsilon}_{\substack{\text{Suppression of }\epsilon\\ \text{by }A_1}}-\underbrace{d_\epsilon\epsilon}_{\text{decay of }\epsilon}. \quad (1)$$

Since treatment pulses are introduced at $t=0$ in the simulation framework, the initial value of ϵ was computed without drug intervention. We further assumed that before treatment, ϵ reaches its quasi–steady state determined by the tumor volume at time zero. This leads to

$$\epsilon(0)=\frac{k_{\text{basal}}}{d_\epsilon}\frac{V(0)}{K_V+V(0)},$$

with $V(0)=100$ representing the tumor volume at the start of the simulation as taken by Nikolopoulou et al., which aligns with experimental observations [14].

2.5. Parameter Estimation

Model parameters were estimated by fitting the models to the experimental tumor volume data using the `lsqnonlin` function in MATLAB R2024a, which minimized the sum of squared errors (SSE) between the model simulation and the data. This process was performed for both models. For the base model, the PD-L1 expression parameter, ϵ, was fitted as a unique constant for each of the six therapies individually. For the final model, the five key parameters governing the dynamics of ϵ from its own differential equation (Equation (1)) were optimized simultaneously across all six experimental datasets. Standard errors from the experiment were not used in the fitting process.

Model performance and complexity were evaluated using the Residual Sum of Squares (RSS) and the Akaike Information Criterion (AIC). The RSS, equivalent to the SSE minimized during fitting, was computed as $\text{RSS} = \sum_{i=1}^{n}(y_i - f(t_i))^2$, where y_i and $f(t_i)$ denote the observed and predicted tumor volumes, respectively. A lower RSS indicates a better fit. The AIC, which penalizes model complexity, was calculated as $\text{AIC} = n\ln(\text{RSS}/n) + 2k$, where k is the number of fitted parameters. A lower AIC score indicates a better balance between a model's goodness of fit and its complexity.

3. Results

3.1. Base Model Limitations Highlight the Need for Dynamic ϵ

To empirically investigate the context-dependent nature of tumor PD-L1 expression, we performed individual fits of the core model where ϵ was treated as a constant parameter, fitted independently for each of the six treatment therapies. This approach allowed us to understand the tumor's adaptive response as different treatments were used. The results from these individual fits demonstrated that the optimal ϵ value varied across treatments. For instance, NHS-muIL12 monotherapy (therapies 2 and 3) led to a substantial increase in the fitted ϵ compared to the Isotype Control (therapy 1), suggesting a tumor counter-adaptation by upregulating PD-L1 in response to enhanced immune stimulation. Conversely, Avelumab monotherapy (therapy 4) resulted in a markedly lower fitted ϵ, indicating a suppression of the tumor's effective PD-L1 expression. These empirical findings provide strong motivation for the subsequent development of more mechanistic representations for ϵ. Model fits are presented in Figure 2 and we show how ϵ varies across therapies.

3.2. Dynamic ϵ Improves Fit and Explanatory Power

The model that included the dynamic ϵ (Equation (1)) successfully fit the full spectrum of experimental outcomes, including the monotherapy responses and the synergistic tumor regression in the low- and high-dose combination therapy Figure 4. The model's ability to accurately capture all six datasets with a single set of parameters demonstrates its robustness and explanatory power. Estimated parameters are shown in Table 1.

Table 1. Additional parameter values used in the dynamic ϵ model. All parameters have units time^{-1}.

Var.	Meaning	Fitted Value
k_{basal}	Basal proliferation rate	30.5441
K_V	PD-L1 Upregulation Sensitivity	50
α_{A_1}	Decay rate induced by Avelumab	38.2653
α_{A_2}	Proliferation induced by NHS-muIL12	643.6397
d_ϵ	Decay rate	0.4409

Furthermore, the simulated trajectory of ϵ itself provides a mechanistic explanation for the observed tumor dynamics. In the NHS-muIL12 monotherapies, the model predicts an early sharp and sustained increase in ϵ, quantitatively simulating the process of adaptive immune resistance. Conversely, in the presence of Avelumab, the model shows a strong suppression of ϵ. This alignment between the model's internal dynamics and the known biological mechanisms validates the model's structure and confirms that the dynamic regulation of PD-L1 is a key determinant of the therapeutic outcome.

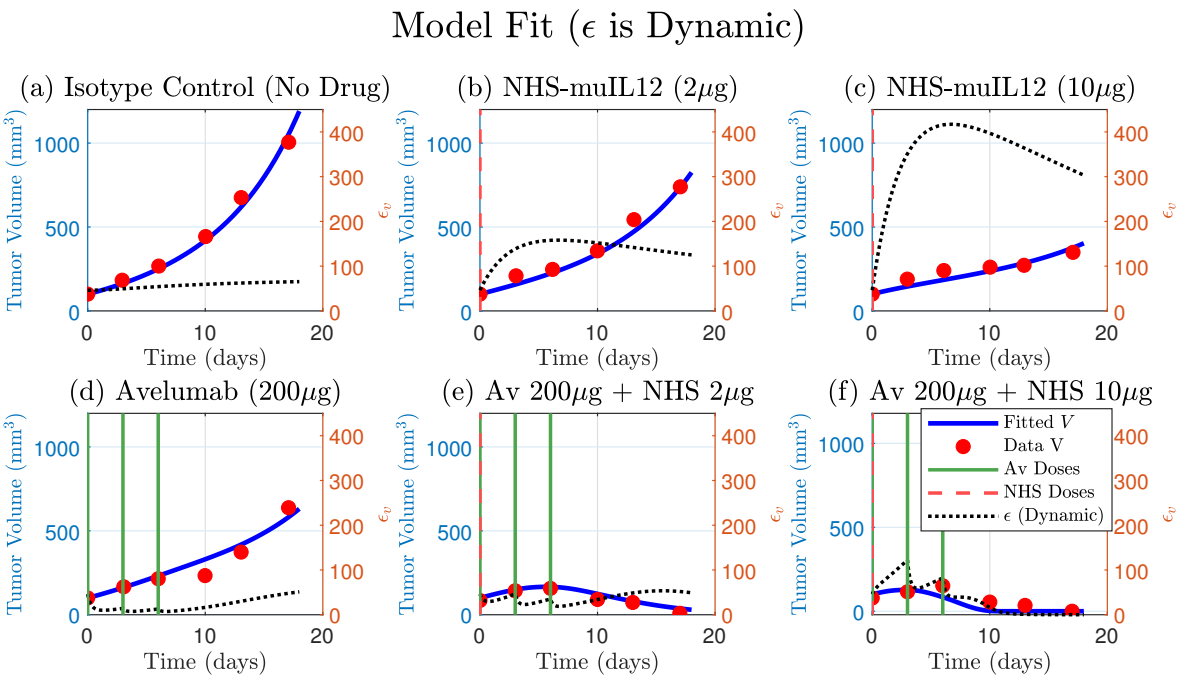


Figure 4. A single set of fitted parameters for the model that includes a dynamic PD-L1 expression (Equation (1)) successfully fits the full spectrum of therapeutic outcomes. The model's simulated tumor volume (blue curve) is plotted against tumor data (red circles) for all six treatments. The model accurately captures the monotherapy responses (panels (**b**–**d**)), the tumor regression in the low- and high-dose combination therapies. The corresponding simulated trajectory ϵ (dashed-black, right y-axis) provides a mechanistic basis for these responses, qualitatively demonstrating adaptive resistance by the tumor. Avelumab and NHS-muIL12 doses are indicated by solid green and dashed vertical lines, respectively. Four parameters were fitted: α_{basal}, α_{A_2}, α_{A_1} and d_ϵ (see Table 1 for values).

3.3. Model Comparisons (RSS and AIC)

The model with constant ϵ was fit independently to each treatment, resulting in six separate parameter sets (one ϵ per treatment). Each treatment scenario contained six data points (36 total). The total AIC reported for this approach is the sum of the six independent fits. In contrast, the model with dynamic ϵ is a single mechanistic framework simultaneously fit to all 36 data points using five global parameters shared across treatments. While AIC values from independent and simultaneous fits are not strictly comparable, the dynamic ϵ model achieved a total AIC only 9 units higher than the combined constant ϵ fits, indicating that it explains all datasets simultaneously with nearly equivalent descriptive accuracy but with one less parameter.

We summarize the residual sum of squares (RSS) and AIC values below, with detailed results provided in Table 2. Both modeling approaches support the central hypothesis that ϵ is not fixed, but varies across treatment conditions due to tumor evolution and adaptation. The constant ϵ model yielded a total RSS of 3.52×10^4 and a summed AIC of 259.8. The dynamic ϵ model achieved an overall RSS of 4.76×10^4 and an AIC of 268.8.

When broken down by treatment, the constant ϵ model generally achieved lower residuals (Table 2). For example, in the low-dose combination treatment, the residual error decreased substantially under the constant ϵ formulation (739.9 vs. 2330.5), and in the high-dose combination therapy, it was reduced by more than half (3240.4 vs. 6474.1). The one notable exception was the Avelumab-only treatment, where the dynamic ϵ model produced a better fit (RSS = 14,853 vs. 18,396).

Table 2. Model comparison between the constant and dynamic ϵ formulations across experimental conditions. Residual sum of squares (RSS) and Akaike information criterion (AIC) are reported, with lower values indicating better fit. The constant ϵ model was fit separately to six data points per therapy (36 total), while the dynamic ϵ model was fit simultaneously to all 36 points to generate metrics for each therapy. The original model uses the updated parameters described in Section 2.3.

Therapy	Original	Constant ϵ		Dynamic ϵ	
	RSS	RSS	AIC	RSS	AIC
(a) Isotype Control (No Drug)	5401	5367.9	42.779	6555.9	51.978
(b) NHS-muIL12 (2 μg)	26,367	5664.4	43.101	8251.0	53.358
(c) NHS-muIL12 (10 μg)	12,332	3240.4	39.750	6474.1	51.903
(d) Avelumab (200 μg)	27,188	18,396.0	50.169	14,853.0	56.885
(e) Av (200 μg) + NHS (2 μg)	249,770	739.9	30.889	2330.5	45.772
(f) Av (200 μg) + NHS (10 μg)	9094.4	1762.4	36.096	9161.8	53.986
Total/Global Fit	3.30×10^5	3.52×10^4	259.84	4.76×10^4	268.75

Overall, these results confirm that both approaches are consistent with the hypothesis of a changing ϵ from a cancer that is adapting to treatment scenarios. The constant ϵ model achieves higher descriptive accuracy, because it fits each treatment independently. While the dynamic ϵ model attains comparable performance through a single mechanistic parameterization that captures shared dynamics across all therapies.

3.4. Model Conclusions Are Robust to Parameter Uncertainty

To assess the model's robustness to potential variability in fixed, literature-derived parameters, we performed a local sensitivity analysis. We systematically perturbed the seven parameters (k_{basal}, α_{A_i}, K_{A_i}, d_ϵ, K_V) and the two fixed pharmacokinetic (PK) parameters (d_{A1}, d_{A2}) by $\pm$25% and re-simulated all six treatment modes (summary results in Supplementary Figure S2). This analysis revealed that Mode 6, the high-dose combination, was the most sensitive to parameters.

We therefore performed a focused time-course analysis on Mode 6, varying the parameters for ϵ production (α_{A_2}), ϵ blockade (α_{A_1}), Avelumab binding (K_{A_1}), and Avelumab clearance (d_{A_1}). The results, shown in Figure 5, demonstrate that while the model is sensitive to these key mechanistic parameters, the qualitative outcome of tumor elimination is not compromised by a $\pm$25% variation. This analysis provides confidence that our model structure is sound and that its core conclusions, namely the necessity of combination therapy to simultaneously stimulate T-cells and block the resulting adaptive resistance, are robust and not an artifact of specific literature-derived parameter choices.

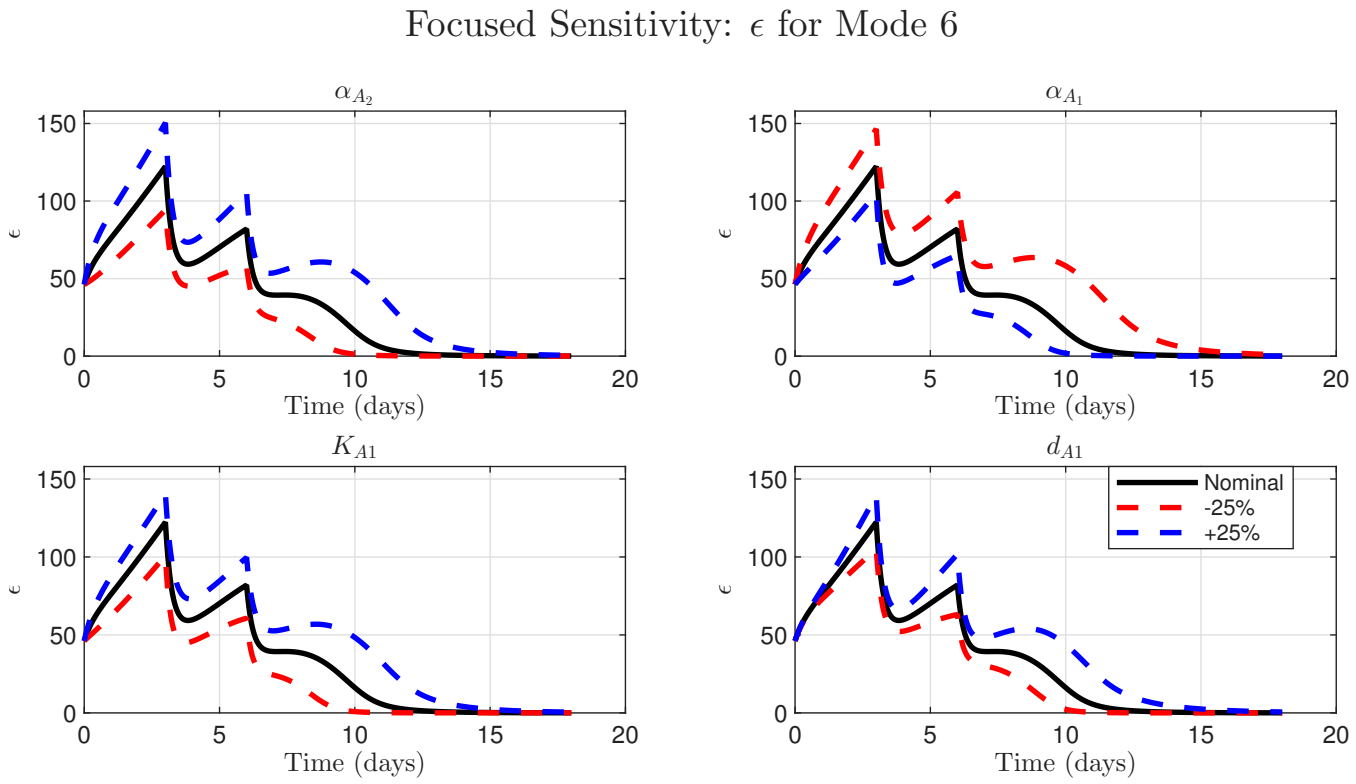


Figure 5. Model conclusions are robust to parameter uncertainty for the high-dose combination (Mode 6). Sensitivity analysis of the simulated time-course of the dynamic ϵ variable from Equation (1). Each subplot compares the nominal simulation (solid black line) to simulations where a single key parameter was perturbed by ±25% (dashed red and blue lines). The parameters investigated are as follows: (**Top Left**) α_{A_2}, the parameter for NHS-muIL12-driven ϵ production; (**Top Right**) α_{A_1}, the parameter for Avelumab-driven ϵ blockade; (**Bottom Left**) K_{A1}, the Avelumab binding affinity; (**Bottom Right**) d_{A1}, the Avelumab clearance rate. In all cases, the qualitative model behavior (the two peaks and eventual decay of ϵ to zero since the tumor is eradicated) is preserved, demonstrating model robustness.

4. Discussion

4.1. Summary of Key Findings

In this study, we developed a mechanistic model that qualitatively explains the complex dynamics of combination therapy first considered by Nikolopoulou et al., which was derived from experimental data [14]. We observed that ϵ was a dynamically changing parameter rather than a constant by fitting it individually across all therapies (Figure 2, bottom panel). This intermediate step improved the fits and provided strong quantitative evidence that the tumor was actively adapting its PD-L1 expression in response to the different therapies. However, this descriptive approach lacked predictive power and motivated the development of a dynamic representation of PD-L1 expression, where ϵ is governed by its own mechanistic differential equation. This provided a balance between predictive power while still improving model fits to data, particularly the non-monotone dynamics found in the low-dose combination therapy; see Figures 2–4. Ultimately, both the dynamic and constant ϵ models supported the hypothesis that ϵ varies across therapies. While the constant ϵ model provided a better overall fit (lower RSS and AIC), the dynamic ϵ model explained treatment-specific effects across all therapies using a single mechanistic rule.

4.2. Interpretation of Model Comparisons

The comparison between the constant and dynamic ϵ models highlights the trade-off between descriptive accuracy and mechanistic insight [26]. The constant ϵ model fits each treatment independently, achieving slightly lower residual error, because each dataset has its own parameter value. This flexibility improves numerical fit, but provides no shared biological explanation of why ϵ is changing. In contrast, the dynamic ϵ model uses a single mechanistic framework across all treatments. Although we report AIC for reference, it is not formally meaningful to compare the total AIC of six independent fits to that of a single joint fit. Despite this, it reproduces the data with only a modest increase in AIC (ΔAIC = 9), demonstrating that a common adaptive mechanism can largely explain the observed treatment-specific differences. This apparent paradox illustrates a broader modeling principle: higher descriptive accuracy does not necessarily imply greater explanatory power. The dynamic ϵ model achieves nearly the same fit as six independent models while providing greater parsimony, mechanistic insight, and predictive potential across treatment conditions.

4.3. Adaptive Resistance via PD-L1 Upregulation

The final model provides a quantitative validation for the biological mechanism of adaptive immune resistance. Our simulations of NHS-muIL12 monotherapy accurately predict a dramatic increase in ϵ, leading to T-cell suppression and subsequent treatment failure. This directly reflects the IFN-γ-dependent PD-L1 upregulation demonstrated experimentally by Fallon et al., who conclusively proved this link using IFN-γ knockout mice [35]. The differential equation governing ϵ in our model includes the parameter α_{NHS} which explicitly captures this process. We chose to link PD-L1 upregulation directly to the presence of NHS-muIL12 rather than explicitly modeling the intermediate IFN-γ step, as this simpler formulation is more robust and avoids further parameter identifiability issues while still capturing the essential dynamics.

Our finding that dynamic PD-L1 expression is a critical determinant of therapeutic outcome is complemented by the work of Lai and Yu [41]. Through a stability analysis of a similar model that included T-cell exhaustion, they independently identified tumor PD-L1 expression as a sensitive parameter that governs the bistability of tumor-free and tumorous states, reinforcing its central role in mediating immune escape.

4.4. Model Generalizability and Cross-Validation

A central test of a mechanistic model's validity is its ability to generalize across distinct tumor contexts, even when a subset of biologically tumor-dependent parameters is refitted. To evaluate this, we applied our model to the independent MC38 tumor dataset from the same study [14]. This experiment included $n = 8$ mice per group and tested responses to NHS-muIL12 (2 μg or 10 μg) and Avelumab (400 μg), administered either as monotherapies or in combination. The MC38 dataset exhibits a treatment response profile distinct from EMT-6, providing a rigorous test of the model's mechanistic framework.

For MC38, we refitted only the five parameters, following the same two-step estimation procedure used for EMT-6, while keeping the remaining parameters unchanged. As shown in Figure 6, the model with these refitted parameters qualitatively reproduces the complex response dynamics across all six treatment arms.

We also fitted the simpler constant-ϵ model to the MC38 data. This analysis reproduced the same biological trends observed in EMT-6: ϵ increased with NHS-muIL12 dose, decreased for Avelumab monotherapy, and rose again with combination therapy (consistent with Figure 2). The dynamic ϵ model shows a similar trend when averaged over time (Figure 6).

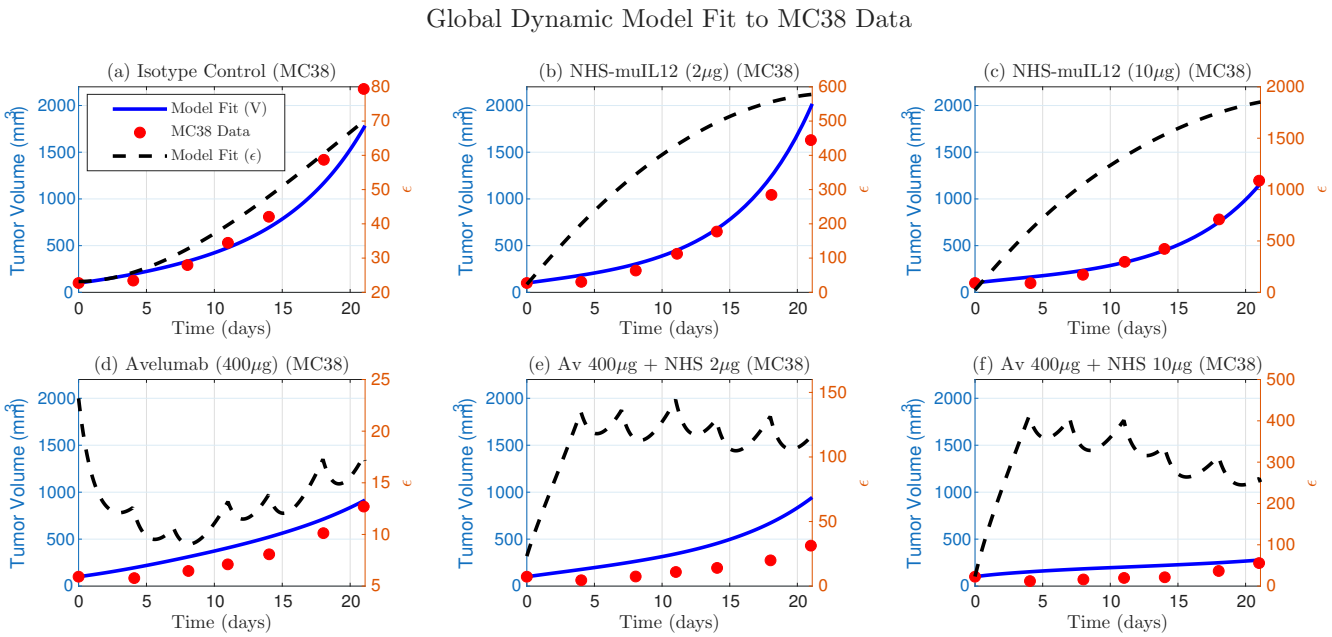


Figure 6. Global dynamic model fit to the independent MC38 dataset. The dynamic ϵ model, with refitted parameters ($k_{\text{basal}} = 12.64$, $\alpha_{A_1} = 3.72$, $\alpha_{A_2} = 1990.17$, $d_\epsilon = 0.10$, $K_V = 462.70$), captures the treatment dynamics (blue lines) against experimental data (red dots). Predicted ϵ trajectories, representing functional immunosuppressive strength, are shown as dashed black lines.

These results provide strong evidence that the core mechanistic structure, which describes the interplay between T-cell stimulation, adaptive regulation of functional immunosuppressive strength, and drug-mediated reduction of immunosuppression, remains consistent across tumor types. Differences in treatment outcomes between EMT-6 and MC38 can be quantitatively explained by tumor-specific variations in the rates governing T-cell activation and the dynamics of immunosuppressive strength, rather than by changes to the underlying mechanism. The two validated parameter sets provide a model-based framework for understanding the key factors that differentiate treatment success from failure.

4.5. Alternative Mechanisms and Model Limitations

While our model mechanistically attributes treatment failure to the upregulation of the tumor's PD-L1 expression, another biologically plausible mechanism that could explain the observed relapse is T-cell exhaustion in the tumor microenvironment [42,43]. This phenomenon describes a state of T-cell dysfunction that arises from chronic exposure to tumor antigens. Over time, persistent stimulation can lead to a progressive loss of effector functions, such as the ability to proliferate and secrete cytotoxic molecules, even if the PD-1/PD-L1 blockade is maintained [42]. In the context of our model, this would mean that even with a dynamically changing PD-L1 expression (ϵ), the T-cell population (T) itself would become less effective at killing tumor cells. Future iterations of this model could incorporate T-cell exhaustion by making the T-cell death rate (d_T) a function of a proxy for cumulative antigen exposure, or by adding a separate, "exhausted" T-cell population. Distinguishing the relative contributions of adaptive resistance via PD-L1 upregulation versus intrinsic T-cell exhaustion remains a key challenge and an important direction for future investigation.

An alternative interpretation of our model's dynamic ϵ is that it represents the consequence of clonal selection within a heterogeneous tumor [44]. While the biological reality is likely a continuous spectrum of resistant cells, it is simpler to conceptualize this as a mixture of two populations: therapy-sensitive cells (with a low potential for PD-L1 expres-

sion) and a pre-existing sub-clone of intrinsically resistant cells (with a high capacity for PD-L1 upregulation) [45–50]. The immunotherapy then acts as a strong, selective pressure, efficiently eliminating the sensitive population at one end of the spectrum. This allows the more resistant clones, which were initially a small fraction of the tumor, to survive and proliferate, eventually shifting the entire population's distribution towards higher resistance. As this evolutionary process occurs, the average PD-L1 expression potential of the whole tumor increases, which is precisely what our model captures through the dynamic increase in the single epsilon parameter under NHS-muIL12 therapy (Figure 2). Therefore, our model's framework can be seen as an effective representation of the bulk tumor dynamics that result from this underlying process of clonal evolution across a resistance spectrum.

5. Conclusions

This study demonstrates the power of an iterative mathematical modeling approach to quantitatively dissect the mechanisms of adaptive resistance in combination immunotherapy. By showing that incorporating therapy-dependent, nonconstant regulation of PD-L1 enabled a biologically grounded mechanism to reproduce experimental observations, we formulated PD-L1 tumor expression as a dynamic variable (ϵ), thereby providing a mechanistic basis for both therapeutic synergy and treatment failure within the original model. This work builds onto a robust in silico platform that can be leveraged to design and test novel therapeutic strategies to overcome the challenge of tumor immune escape.

Supplementary Materials: The following supporting information can be downloaded at https://www.mdpi.com/article/10.3390/cancers17233803/s1. Table S1: Model Comparison for EMT-6 Data; Figure S1: Dynamic Model Fit to 8-Mouse Composite Mean; Figure S2: Comprehensive Sensitivity Analysis (Epsilon).

Author Contributions: Conceptualization, B.P., D.D., A.K. (Aigerim Kalizhanova), A.K. (Ardak Kashkynbayev) and Y.K.; methodology, B.P., A.K. (Aigerim Kalizhanova) and Y.K.; software, B.P. and A.K. (Aigerim Kalizhanova); validation, B.P., D.D. and A.K. (Aigerim Kalizhanova); formal analysis, B.P.; investigation, A.K. (Aigerim Kalizhanova), A.K. (Ardak Kashkynbayev), A.T., B.P., D.D. and Y.K.; resources, A.K. (Ardak Kashkynbayev), B.P. and Y.K.; data curation, B.P. and D.D.; writing—original draft preparation, B.P.; writing—review and editing, A.K. (Aigerim Kalizhanova), A.K. (Ardak Kashkynbayev), A.T., B.P., D.D. and Y.K.; visualization, A.T. and B.P.; supervision, A.K. (Ardak Kashkynbayev) and Y.K.; project administration, B.P. and Y.K.; funding acquisition, A.K. (Ardak Kashkynbayev), B.P. and Y.K. All authors have read and agreed to the published version of the manuscript.

Funding: Aigerim Kalizhanova, Aisha Tursynkozha and Ardak Kashkynbayev were funded in part by the Committee of Science of the Ministry of Science and Higher Education of the Republic of Kazakhstan (Grant No. BR24993094). Y.K. is supported by the U.S. NSF grant DMS-2325146 and DMS-2421258 and US NIH grant 1R01AI192873-01. B.P. is supported by the U.S. NSF grant DMS-2421260 and DMS-2316809 and US NIH grant 1R01AI192873-01.

Institutional Review Board Statement: Not applicable.

Informed Consent Statement: Not applicable.

Data Availability Statement: The data used in this study were digitized from figures in the published work by [14]. The derived dataset generated for this article is available from the corresponding author upon reasonable request, subject to any permissions required by the original copyright holder.

Acknowledgments: We thank the four anonymous reviewers for their thoughtful and constructive feedback, which greatly improved the quality of this manuscript.

Conflicts of Interest: The authors declare no conflicts of interest.

Appendix A

Here, we provide the parameter values that were used for the model fittings.

Table A1. Model parameters, their meanings, values, and references.

Var.	Meaning	Value	Ref.
r	Tumor cell growth rate	$0.213\,\mathrm{day}^{-1}$	[27]
η	Kill rate of tumor cells by T cells	$1\,\mathrm{mm}^{-3}\,\mathrm{day}^{-1}$	[27]
δ	Source of T cell activation	$0.02\,\mathrm{mm}^3/\mathrm{day}$	[27]
$\lambda_{T_{IL12}}$	Activation rate of T cells by IL-12	$4.15\,\mathrm{day}^{-1}$	[32]
K_{TQ}	Inhibition of T cells by PD-1–PD-L1	$1 \times 10^{-13}\,\mathrm{mm}^6$	[27]
K_{A_1}	Dissociation constant of PD-L1–anti-PD-L1	$1 \times 10^{-13}\,\mathrm{mol/L}$	[27]
K_{A_2}	Dissociation constant of PD-L1–anti-PD-L1	$1 \times 7 \times 10^{-14}\,\mathrm{mol/L}$	[27]
d_T	Death rate of T cells	0–$0.5\,\mathrm{day}^{-1}$	[51]
d_{A_1}	Degradation rate of Anti-PD-L1	$0.3726\,\mathrm{day}^{-1}$	[33]
d_{A_2}	Degradation rate of NHS-muIL12	$0.0730\,\mathrm{day}^{-1}$	[34]
ρ_p	Expression level of PD-1	3.19×10^{-7}–8.49×10^{-7}	[32]
ρ_L	Expression level of PD-L1	3.56×10^{-7}–1.967×10^{-6}	[32]
ϵ	PD-L1 expression from tumor	–	fitted
σ	Complex assoc./dissoc. fraction	$0.01\,\mathrm{mm}^{-3}$	[27]
γ_1	Infusion rate of Avelumab	1×10^{-7}–$9 \times 10^{-5}\,\mathrm{g/day}$	[27]
γ_2	Infusion rate of NHS-muIL12	1×10^{-9}–$2 \times 10^{-6}\,\mathrm{g/day}$	[27]
c_1	Conversion constant for A_1	$55^{-1} \times 10^{-7}$–$55^{-1} \times 10^{-6}$	[27]
c_2	Conversion constant for A_2	$75^{-1} \times 10^{-7}$–$75^{-1} \times 10^{-6}$	[27]

References

1. Burrell, R.A.; McGranahan, N.; Bartek, J.; Swanton, C. The causes and consequences of genetic heterogeneity in cancer evolution. *Nature* **2013**, *501*, 338–345. [CrossRef] [PubMed]
2. Gerlinger, M.; McGranahan, N.; Dewhurst, S.M.; Burrell, R.A.; Tomlinson, I.; Swanton, C. Cancer: Evolution Within a Lifetime. *Annu. Rev. Genet.* **2014**, *48*, 215–236. [CrossRef]
3. Vendramin, R.; Litchfield, K.; Swanton, C. Cancer evolution: Darwin and beyond. *EMBO J.* **2021**, *40*, e108389. [CrossRef]
4. Pardoll, D.M. The blockade of immune checkpoints in cancer immunotherapy. *Nat. Rev. Cancer* **2012**, *12*, 252–264. [CrossRef]
5. Schilsky, R.L. Implementing personalized cancer care. *Nat. Rev. Clin. Oncol.* **2014**, *11*, 432–438. [CrossRef]
6. Lin, H.H.; Wei, N.C.; Chou, T.Y.; Lin, C.C.; Lan, Y.T.; Chang, S.C.; Wang, H.S.; Yang, S.H.; Chen, W.S.; Lin, T.C.; et al. Building personalized treatment plans for early-stage colorectal cancer patients. *Oncotarget* **2017**, *8*, 13805–13817. [CrossRef]
7. Han, Y.; Liu, D.; Li, L. PD-1/PD-L1 pathway: Current researches in cancer. *Am. J. Cancer Res.* **2020**, *10*, 727–742. [PubMed]
8. Juneja, V.R.; McGuire, K.A.; Manguso, R.T.; LaFleur, M.W.; Collins, N.; Haining, W.N.; Freeman, G.J.; Sharpe, A.H. PD-L1 on tumor cells is sufficient for immune evasion in immunogenic tumors and inhibits CD8 T cell cytotoxicity. *J. Exp. Med.* **2017**, *214*, 895–904. [CrossRef]
9. Collins, J.M.; Gulley, J.L. Product review: Avelumab, an anti-PD-L1 antibody. *Hum. Vaccines Immunother.* **2019**, *15*, 891–908. [CrossRef] [PubMed]
10. Vaishampayan, U.; Schöffski, P.; Ravaud, A.; Borel, C.; Peguero, J.; Chaves, J.; Morris, J.C.; Kotecki, N.; Smakal, M.; Zhou, D.; et al. Avelumab monotherapy as first-line or second-line treatment in patients with metastatic renal cell carcinoma: Phase Ib results from the JAVELIN Solid Tumor trial. *J. Immunother. Cancer* **2019**, *7*, 275. [CrossRef]
11. Liu, K.; Tan, S.; Chai, Y.; Chen, D.; Song, H.; Zhang, C.W.H.; Shi, Y.; Liu, J.; Tan, W.; Lyu, J.; et al. Structural basis of anti-PD-L1 monoclonal antibody avelumab for tumor therapy. *Cell Res.* **2017**, *27*, 151–153. [CrossRef] [PubMed]
12. Fallon, J.; Tighe, R.; Kradjian, G.; Guzman, W.; Bernhardt, A.; Neuteboom, B.; Lan, Y.; Sabzevari, H.; Schlom, J.; Greiner, J.W. The immunocytokine NHS-IL12 as a potential cancer therapeutic. *Oncotarget* **2014**, *5*, 1869–1884. [CrossRef]
13. Greiner, J.W.; Morillon, Y.M., II; Schlom, J. NHS-IL12, a Tumor-Targeting Immunocytokine. *Immunotargets Ther.* **2021**, *10*, 155–169. [CrossRef]
14. Xu, C.; Zhang, Y.; Rolfe, P.A.; Hernández, V.M.; Guzman, W.; Kradjian, G.; Marelli, B.; Qin, G.; Qi, J.; Wang, H.; et al. Combination Therapy with NHS-muIL12 and Avelumab (anti-PD-L1) Enhances Antitumor Efficacy in Preclinical Cancer Models. *Clin. Cancer Res.* **2017**, *23*, 5869–5880. [CrossRef]
15. Altrock, P.M.; Liu, L.L.; Michor, F. The mathematics of cancer: Integrating quantitative models. *Nat. Rev. Cancer* **2015**, *15*, 730–745. [CrossRef]

16. Phan, T.; Crook, S.M.; Bryce, A.H.; Maley, C.C.; Kostelich, E.J.; Kuang, Y. Review: Mathematical Modeling of Prostate Cancer and Clinical Application. *Appl. Sci.* **2020**, *10*, 2721. [CrossRef]
17. Brady, R.; Enderling, H. Mathematical Models of Cancer: When to Predict Novel Therapies, and When Not to. *Bull. Math. Biol.* **2019**, *81*, 3722–3731. [CrossRef]
18. Rauf, S.; Smirnova, A.; Chang, A.; Liu, Y.; Jiang, Y. Immunogenic Cell Death: The Key to Unlocking the Potential for Combined Radiation and Immunotherapy. *bioRxiv* **2025**. [CrossRef]
19. Kuang, Y.; Nagy, J.D.; Eikenberry, S.E. *Introduction to Mathematical Oncology*; Chapman & Hall/CRC: Boca Raton, FL, USA, 2016.
20. Serre, R.; Benzekry, S.; Padovani, L.; Meille, C.; André, N.; Ciccolini, J.; Barlesi, F.; Muracciole, X.; Barbolosi, D. Mathematical Modeling of Cancer Immunotherapy and Its Synergy with Radiotherapy. *Cancer Res.* **2016**, *76*, 4931–4940. [CrossRef] [PubMed]
21. Bräutigam, K. Optimization of chemotherapy regimens using mathematical programming. *Comput. Ind. Eng.* **2024**, *191*, 110078. [CrossRef]
22. Hahnfeldt, P.; Panigrahy, D.; Folkman, J.; Hlatky, L. Tumor development under angiogenic signaling: A dynamical theory of tumor growth, treatment response, and postvascular dormancy. *Cancer Res.* **1999**, *59*, 4770–4775. [PubMed]
23. Reckell, T.; Nguyen, K.; Phan, T.; Crook, S.; Kostelich, E.J.; Kuang, Y. Modeling the synergistic properties of drugs in hormonal treatment for prostate cancer. *J. Theor. Biol.* **2021**, *514*, 110570. [CrossRef]
24. Meade, W.; Weber, A.; Phan, T.; Hampston, E.; Resa, L.F.; Nagy, J.; Kuang, Y. High Accuracy Indicators of Androgen Suppression Therapy Failure for Prostate Cancer—A Modeling Study. *Cancers* **2022**, *14*, 4033. [CrossRef]
25. Phan, T.; Weber, A.; Bryce, A.H.; Kuang, Y. The prognostic value of androgen to PSA ratio in predictive modeling of prostate cancer. *Med. Hypotheses* **2023**, *176*, 111084. [CrossRef]
26. Glasser, J.W.; Feng, Z. Mechanistic models are hypotheses: A perspective. *Math. Biosci.* **2025**, *383*, 109419. [CrossRef]
27. Nikolopoulou, E.; Eikenberry, S.E.; Gevertz, J.L.; Kuang, Y. Mathematical modeling of an immune checkpoint inhibitor and its synergy with an immunostimulant. *Discret. Contin. Dyn. Syst. B* **2021**, *26*, 2133–2159. [CrossRef]
28. Sarapata, E.A.; de Pillis, L.G. A Comparison and Catalog of Intrinsic Tumor Growth Models. *Bull. Math. Biol.* **2014**, *76*, 2010–2024. [CrossRef]
29. Kuznetsov, V.A.; Makalkin, I.A.; Taylor, M.A.; Perelson, A.S. Nonlinear dynamics of immunogenic tumors: Parameter estimation and global bifurcation analysis. *Bull. Math. Biol.* **1994**, *56*, 295–321. [CrossRef] [PubMed]
30. Kirschner, D.; Panetta, J.C. Modeling immunotherapy of the tumor-immune interaction. *J. Math. Biol.* **1998**, *37*, 235–252. [CrossRef] [PubMed]
31. PlotDigitizer: Version 3.1.6. 2025. Available online: https://plotdigitizer.com (accessed on 18 June 2025).
32. Lai, X.; Friedman, A. Combination therapy of cancer with cancer vaccine and immune checkpoint inhibitors: A mathematical model. *PLoS ONE* **2017**, *12*, e0178479. [CrossRef]
33. Zalba, S.; Contreras-Sandoval, A.M.; Martisova, E.; Debets, R.; Smerdou, C.; Garrido, M.J. Quantification of Pharmacokinetic Profiles of PD-1/PD-L1 Antibodies by Validated ELISAs. *Pharmaceutics* **2020**, *12*, 595. [CrossRef] [PubMed]
34. Unverdorben, F.; Richter, F.; Hutt, M.; Seifert, O.; Malinge, P.; Fischer, N.; Kontermann, R.E. Pharmacokinetic properties of IgG and various Fc fusion proteins in mice. *mAbs* **2016**, *8*, 120–128. [CrossRef]
35. Fallon, J.K.; Vandeveer, A.J.; Schlom, J.; Greiner, J.W. Enhanced antitumor effects by combining an IL-12/anti-DNA fusion protein with avelumab, an anti-PD-L1 antibody. *Oncotarget* **2017**, *8*, 20558–20571. [CrossRef]
36. Liao, K.L.; Watt, K.D. Mathematical modeling for the combination treatment of IFN-γ and anti-PD-1 in cancer immunotherapy. *Math. Biosci.* **2022**, *353*, 108911. [CrossRef]
37. Wang, X.; Teng, F.; Kong, L.; Yu, J. PD-L1 expression in human cancers and its association with clinical outcomes. *Oncotargets Ther.* **2016**, *9*, 5023–5039. [CrossRef]
38. Zhao, Y.; Shi, Z.; Xie, Y.; Li, N.; Chen, H.; Jin, M. The association between PD-1/PD-L1 expression and clinicopathological features in sarcomatoid renal cell carcinoma. *Asian J. Surg.* **2024**, *47*, 163–168. [CrossRef] [PubMed]
39. Yu, X.; Li, W.; Young, K.H.; Li, Y. Posttranslational Modifications in PD-L1 Turnover and Function: From Cradle to Grave. *Biomedicines* **2021**, *9*, 1702. [CrossRef] [PubMed]
40. Lemma, E.Y.; Letian, A.; Altorki, N.K.; McGraw, T.E. Regulation of PD-L1 Trafficking from Synthesis to Degradation. *Cancer Immunol. Res.* **2023**, *11*, 866–874. [CrossRef]
41. Lai, X.; Yu, T. Modeling Combination Therapies and T Cell Exhaustion Dynamics in the Tumor Under Immune Checkpoint Blockade. *Bull. Math. Biol.* **2025**, *87*, 128. [CrossRef]
42. Zhang, Z.; Liu, S.; Zhang, B.; Qiao, L.; Zhang, Y. T Cell Dysfunction and Exhaustion in Cancer. *Front. Cell Dev. Biol.* **2020**, *8*, 17. [CrossRef]
43. Pauken, K.E.; Wherry, E.J. Overcoming T cell exhaustion in infection and cancer. *Trends Immunol.* **2015**, *36*, 265–276. [CrossRef] [PubMed]

44. Gniadek, T.J.; Li, Q.K.; Tully, E.; Chatterjee, S.; Nimmagadda, S.; Gabrielson, E. Heterogeneous expression of PD-L1 in pulmonary squamous cell carcinoma and adenocarcinoma: Implications for assessment by small biopsy. *Mod. Pathol.* **2017**, *30*, 530–538. [CrossRef]
45. Portz, T.; Kuang, Y.; Nagy, J.D. A clinical data validated mathematical model of prostate cancer growth under intermittent androgen suppression therapy. *AIP Adv.* **2012**, *2*, 011002. [CrossRef]
46. Portz, T.; Kuang, Y. A mathematical model for the immunotherapy of advanced prostate cancer. In Proceedings of the BIOMAT 2012—International Symposium on Mathematical and Computational Biology, Tempe, AZ, USA, 6–10 November 2012; World Scientific: Singapore, 2013; pp. 70–85. [CrossRef]
47. Baez, J.; Kuang, Y. Mathematical Models of Androgen Resistance in Prostate Cancer Patients under Intermittent Androgen Suppression Therapy. *Appl. Sci.* **2016**, *6*, 352. [CrossRef]
48. Phan, T.; He, C.; Martinez, A.; Kuang, Y.; Phan, T.; He, C.; Martinez, A.; Kuang, Y. Dynamics and implications of models for intermittent androgen suppression therapy. *Math. Biosci. Eng.* **2019**, *16*, 187–204. [CrossRef] [PubMed]
49. Phan, T.; Nguyen, K.; Sharma, P.; Kuang, Y. The Impact of Intermittent Androgen Suppression Therapy in Prostate Cancer Modeling. *Appl. Sci.* **2019**, *9*, 36. [CrossRef]
50. Everett, R.A.; Packer, A.M.; Kuang, Y. Can Mathematical Models Predict the Outcomes of Prostate Cancer Patients Undergoing Intermittent Androgen Deprivation Therapy? *Biophys. Rev. Lett.* **2014**, *9*, 173–191. [CrossRef]
51. Nikolopoulou, E.; Johnson, L.; Harris, D.; Nagy, J.; Stites, E.; Kuang, Y. Tumour-immune dynamics with an immune checkpoint inhibitor. *Lett. Biomath.* **2018**, *5*, S137–S159. [CrossRef]

Disclaimer/Publisher's Note: The statements, opinions and data contained in all publications are solely those of the individual author(s) and contributor(s) and not of MDPI and/or the editor(s). MDPI and/or the editor(s) disclaim responsibility for any injury to people or property resulting from any ideas, methods, instructions or products referred to in the content.